

Detecting atmospheric neutrino oscillations in the ATLAS detector at CERN

Joachim Kopp^a and Manfred Lindner^b

*Max-Planck-Institut für Kernphysik
Postfach 10 39 80, D-69026 Heidelberg, Germany*

(Dated: November 15, 2018)

We discuss the possibility to study oscillations of atmospheric neutrinos in the ATLAS experiment at CERN. Due to the large total detector mass, a significant number of events is expected, and during the shutdown phases of the LHC, reconstruction of these events will be possible with very good energy and angular resolutions, and with charge identification. We argue that 500 live days of neutrino running could be achieved, and that a total of ~ 160 contained ν_μ events and ~ 360 upward going muons could be collected during this time. Despite the low statistics, the excellent detector resolution will allow for an unambiguous confirmation of atmospheric neutrino oscillations and for measurements of the leading oscillation parameters. Though our detailed simulations show that the sensitivity of ATLAS is worse than that of dedicated neutrino experiments, we demonstrate that more sophisticated detectors, e.g. at the ILC, could be highly competitive with upcoming superbeam experiments, and might even give indications for the mass hierarchy and for the value of θ_{13} .

PACS numbers: 14.60.Pq, 13.15.+g

1. INTRODUCTION

Neutrino oscillation physics is entering the era of precision measurements, and a plethora of new dedicated experiments are being designed, or already under construction. The most widely discussed technologies are reactor experiments [1, 2], superbeams [3, 4], advanced atmospheric neutrino detectors [5, 6], beta beams [7, 8], and neutrino factories [9, 10]. In this article, we entertain the possibility to use the ATLAS detector at CERN to study oscillations of atmospheric neutrinos, an idea which has first been brought up by F. Vannucci [11, 12]. A significant number of atmospheric neutrino interactions will take place in the 4 kt hadronic calorimeter of ATLAS, and can be reconstructed with excellent energy and angular resolution during phases where the LHC is not running at full luminosity. Moreover, the magnetic field will allow for the discrimination between neutrinos and anti-neutrinos.

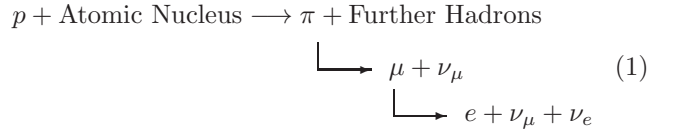
To study the physics that can be done with these event, we have developed a code that allows for the simulation of event spectra, taking into account a full three-flavor treatment of neutrino oscillations, the finite energy and angular resolutions of the experiment, and the detector geometry. To derive high-level results, such as parameter sensitivities, from the simulated data, we use a χ^2 analysis including systematical uncertainties, parameter correlations, and degeneracies.

The paper is organized as follows: After briefly reviewing the physics of atmospheric neutrinos in Sec. 2, we discuss the capabilities of ATLAS to detect atmospheric neutrinos in Sec. 3. We then describe the technical de-

tails of our simulations in Sec. 4, and present the results for the sensitivity to the leading atmospheric oscillation parameters, to the mass hierarchy, and to other three-flavor effects, in Sec. 5. Our conclusions will be presented in Sec. 6.

2. OSCILLATIONS OF ATMOSPHERIC NEUTRINOS

Atmospheric neutrinos are produced by interactions of cosmic rays with the atmosphere at a height of around 10 to 20 km above ground. The main production reaction is



Due to strong $\nu_\mu \rightarrow \nu_\tau$ oscillations, the flux of upward going neutrinos is significantly lower than that of downward going neutrinos. This leading oscillation effect has been unambiguously detected experimentally [13, 14, 15, 16, 17]. In contrast, subleading three-flavor effects, such as $\nu_\mu \rightarrow \nu_e$ oscillations driven by θ_{13} and Δm_{31}^2 , are very hard to detect with atmospheric neutrinos because the flux ratio $(\nu_\mu + \bar{\nu}_\mu)/(\nu_e + \bar{\nu}_e) \approx 2$ (cf. Eq. (1)), in combination with the close-to-maximal value of θ_{23} leads to a cancellation of $\nu_\mu \rightarrow \nu_e$ and $\nu_e \rightarrow \nu_\mu$ oscillations [18].

Atmospheric neutrinos cover a wide range of energies, but their flux decreases rapidly for $E \gtrsim 3$ GeV. The distances travelled by them before detection range up to 12,742 km, the diameter of the Earth, for upward going neutrinos. Detailed calculations of the atmospheric neutrino fluxes have been performed by Honda et al. [19],

^aEmail: jkopp@mpi-hd.mpg.de

^bEmail: lindner@mpi-hd.mpg.de

Battistoni et al. [20, 21], and Barr et al. [22]. In our study, we will use the Honda fluxes [19].

ATLAS will be sensitive mainly to the leading $\nu_\mu \rightarrow \nu_\tau$ oscillations, but due to the difficulties associated with the reconstruction of ν_τ interactions, the most important oscillation channel will be $\nu_\mu \rightarrow \nu_\mu$ disappearance. Neglecting subleading effects driven by Δm_{21}^2 , the corresponding oscillation probability in matter is given by [23]:

$$P_{\mu\mu} = 1 - \sin^4 \theta_{23} \sin^2 2\theta_{13}^m \sin^2 C_{13} \Delta - \frac{1}{2} \sin^2 2\theta_{23} [1 - \cos(1+A)\Delta \cos C_{13} \Delta + \cos 2\theta_{13}^m \sin(1+A)\Delta \sin C_{13} \Delta] \quad (2)$$

Here, we have used the notation from [23]: $\Delta = \Delta m_{31}^2 L/4E$ is the oscillation phase, $A = 2EV/\Delta m_{31}^2$ describes matter effects, $\sin 2\theta_{13}^m = C_{13}^{-1} \sin 2\theta_{13}$ is the mixing angle in matter, and C_{13} is given by $C_{13} = [\sin^2 2\theta_{13} + (\cos 2\theta_{13} - A)^2]^{1/2}$. The first line in Eq. (2) describes the disappearance due to matter-enhanced $\nu_\mu \rightarrow \nu_e$ oscillations, while the other terms correspond to $\nu_\mu \rightarrow \nu_\tau$ oscillations. A generic three-flavor effect is the strong influence of matter on the $\nu_\mu \rightarrow \nu_\mu$ and $\nu_\mu \rightarrow \nu_\tau$ channels in some regions of the parameter space [24, 25]. In the vacuum case, i.e. for $A = 0$, $C_{13} = 1$, and $\theta_{13}^m = \theta_{13}$, Eq. (2) reduces to

$$P_{\mu\mu} = 1 - [\sin^4 \theta_{23} \sin^2 2\theta_{13} - \cos^2 \theta_{13} \sin^2 2\theta_{23}] \sin^2 \Delta, \quad (3)$$

i.e. to two-flavor oscillations with a mixing angle close to θ_{23} . For the neutrino oscillation parameters, we adopt the following best-fit values in our simulations (see e.g. [26, 27, 28, 29]):

$$\begin{aligned} \sin^2 2\theta_{12} &= 0.79, \\ \sin^2 2\theta_{13} &= 0.12, \\ \sin^2 2\theta_{23} &= 1.0, \\ \delta_{\text{CP}} &= 0.0, \\ \Delta m_{21}^2 &= 8.1 \cdot 10^{-5} \text{ eV}^2, \\ \Delta m_{31}^2 &= 2.2 \cdot 10^{-3} \text{ eV}^2. \end{aligned} \quad (4)$$

3. RECONSTRUCTION OF NEUTRINO INTERACTIONS IN ATLAS

The ATLAS detector at CERN has an onion shell structure, similar to that of most other modern collider experiments: The inner high-resolution tracking detectors are surrounded by the electromagnetic and hadronic calorimeters, large superconducting magnets, and a muon tracking system [30]. ATLAS has a total mass of 7 kt, but part of it is attributed to the non-active support structure of the experiment. Reconstruction of neutrino interactions will only be possible if the energy and direction of the secondary charged lepton can

be seen, and for a good energy and angular resolution, it is desirable to also reconstruct the energies of the other interaction products. For ν_μ interactions, this requires the interaction to take place inside the 4 kt hadronic calorimeter, so that the muons will travel through the whole muon system. Furthermore, the neutrino must have sufficient energy to yield a sizeable signal. We estimate that a threshold of 1.5 GeV should be realistic. For ν_e and ν_τ , the track of the secondary charged lepton can only be seen with good resolution if the interaction takes place in the inner tracking detectors, which, however, have negligible mass. Energy reconstruction for ν_e and ν_τ should in principle be possible also for interactions taking place further outside, but the resolution would be quite poor since only information from the hadronic calorimeter could be used. Therefore, we do not take ν_e and ν_τ into account at all. We do, however, include so-called upward going muons, i.e. muons created by neutrino interactions in the rock below the detector. More precisely, we consider muons coming from the zenith angle range $-1 \leq \cos \theta \leq -0.1$ to be induced by neutrinos. Note that ATLAS, being a magnetized detector, is able to determine the muon charge and can thus discriminate between neutrinos and anti-neutrinos.

A very important issue for the detection of atmospheric neutrinos in ATLAS is triggering. The characteristic signature of an atmospheric neutrino is a high-energy charged lepton track originating from a vertex inside the detector, without any visible ingoing particle. During normal LHC operation at full luminosity, such signals will be cloaked by the pile-up of pp interaction products, and even if they could be seen, they might still be confused with decay products of neutral hadrons. Besides, the ATLAS trigger will only be sensitive during the bunch crossings, because the time between them is required to read out the accumulated data. For these reasons, ATLAS can be used for neutrino physics only during the ~ 200 days per year where the LHC is not running in collider mode [31]. This number arises from the 14 week winter shutdown, and from regular short maintenance shutdowns throughout the year. Moreover, even during LHC operation, the pp interaction rate in the detector will be sufficiently low during the ramp-up and ramp-down phases. Of course, also the ATLAS detector will require maintenance, so that only part of the aforementioned time windows will be available for neutrino physics. If ~ 100 days of neutrino running per year are feasible, this would yield ~ 160 contained events and ~ 360 upward going muons within 5 years. We will show in Sec. 5 that this is sufficient to detect neutrino oscillations and to perform measurements of the oscillation parameters.

Note that the number of neutrino interactions expected in CMS should be even larger than that in ATLAS, since CMS has a total mass of 12 kt. [32]. However, most of this mass is concentrated in the massive iron return yokes of the magnet, so that all non-muonic interaction products will be scattered several times before reaching the active

detector components. This will inhibit a reliable reconstruction of the primary neutrino properties, and hence we will not consider CMS further in this article.

Since the leading oscillation channel for atmospheric neutrinos is $\nu_\mu \rightarrow \nu_\tau$, and the τ has a 17% chance of decaying into $\mu\nu_\mu\nu_\tau$ [33], one has to ask the question whether ν_τ interactions, followed by a leptonic τ decay, can be clearly separated from simple charged current ν_μ interactions. However, this should be possible, since typically, the muon from the τ decay will have a relatively low energy, which is most probably below the threshold used in the analysis.

4. SIMULATION OF ATMOSPHERIC NEUTRINOS

To study the prospects of doing neutrino oscillation physics with ATLAS, we have developed a simulation code for the calculation of event rates as a function of the neutrino energy and zenith angle, and for the χ^2 analysis of the simulated data. We obtain the binned event rates by folding the initial neutrinos fluxes $\Phi_{f'}(E_\nu^k, L(\theta_\nu^l))$, [19], the three-flavor oscillation probabilities in matter $P(f' \rightarrow f, E_\nu^k, L(\theta_\nu^l), \vec{\Theta})$, the cross sections $\sigma_f(E_\nu^k)$ [34, 35], and a detector response function $\tilde{R}^{ij}(E_\nu^k, \theta_\nu^l)$ according to the formula

$$N_f^{ij} = \mathcal{N} \sum_{k,l} \tilde{R}^{ij}(E_\nu^k, \theta_\nu^l) \cdot \sigma_f(E_\nu^k) \cdot \sum_{f'=e,\mu,\tau} P(f' \rightarrow f, E_\nu^k, L(\theta_\nu^l), \vec{\Theta}) \Phi_{f'}(E_\nu^k, L(\theta_\nu^l)).$$

In this expression, E_ν^k and θ_ν^l denote the neutrino energy and zenith angle at the sampling point with indices (k, l) , while (i, j) stands for the binning used in the analysis. The number of bins is roughly chosen according to the energy and angular resolutions (see Tab. I).¹ $L(\theta_\nu^l)$ is the distance travelled by neutrinos coming from the direction θ_ν^l , and $\vec{\Theta}$ represents the vector of oscillation parameters (including the matter potential), i.e. $\vec{\Theta} = (\theta_{12}, \theta_{13}, \theta_{23}, \delta_{\text{CP}}, \Delta m_{21}^2, \Delta m_{31}^2, V)$. The cross sections used in our code cover an energy range from 100 MeV to 1 TeV. For neutrinos with higher energies (up to 10 TeV), which can contribute only to the upward going muon sample, we extrapolate the cross sections by making the assumption that $\sigma(E)/E$ is constant at such high energies. We only use total charged current cross sections. The detector response function $\tilde{R}^{ij}(E_\nu^k, \theta_\nu^l)$ determines which fraction of neutrinos with

initial energy E_ν^k and zenith angle θ_ν^l is reconstructed into bin (i, j) . Since the detector response to neutrinos has not been studied in full detector Monte Carlo simulations yet, we resort to approximating \tilde{R} by a double Gaussian resolution function, multiplied with an efficiency factor $\epsilon(E_\nu, \theta_\nu)$:

$$\tilde{R}^{ij}(E_\nu^k, \theta_\nu^l) = \epsilon(E_\nu, \theta_\nu^l) \cdot \frac{1}{Z_E} \exp\left(-\frac{(E_r^i - E_\nu)^2}{2\sigma_E^2(E_\nu)}\right) \cdot \frac{1}{Z_\alpha} \int_0^{2\pi} d\phi_r \exp\left(-\frac{\alpha^2(\theta_r^j, \phi_r, \theta_\nu^l)}{2\sigma_\alpha^2(E_\nu)}\right).$$

Here, $\sigma_E(E_\nu)$ and $\sigma_\alpha(E_\nu)$ denote the energy and angular resolutions, respectively. $\alpha(\theta_r^j, \phi_r, \theta_\nu^l)$ is the angle between the initial neutrino direction, parameterized by the zenith angle θ_ν^l , and the reconstructed direction, which is defined by the zenith and azimuthal angles θ_r^j and ϕ_r ; Z_E and Z_α are normalization factors which ensure that the total number of events is conserved in the ‘‘smearing’’ of the spectrum. Due to lack of Monte Carlo results on the reconstruction efficiency in ATLAS, we omit $\epsilon(E_\nu, \theta_\nu)$ for contained events. For upward going muons, we use ϵ to scale the flux according to the target volume, which varies with energy and zenith angle (see appendix A for details).

For the resolutions, we use estimates based on the experience of the Super-Kamiokande collaboration [15, 36] and on the information from the ATLAS proposal [30]. In Super-Kamiokande, where only the secondary muon is seen, the energy resolution for contained Multi-GeV events is 17%, and the angular resolution is 17° above 1.5 GeV. The ATLAS calorimeter measures the full deposited energy with a resolution of order $\sigma_E/E \sim 50\%/\sqrt{E/\text{GeV}}$, while the muon system has an energy resolution on the per cent level. The angular resolution of the muon system is excellent because track reconstruction is possible, while the directional information from the hadronic calorimeter is severely limited by its rough segmentation. We will assume that the excellent muon reconstruction, in conjunction with the information from the hadronic calorimeter, will yield an overall neutrino energy resolution of 5%, and an angular resolution of 7° for contained events. Let us emphasize that these numbers are only estimates, and for more reliable numbers, detailed detector Monte Carlo simulations are indispensable. For upward going muons, no energy reconstruction is possible, and the angular resolution is essentially given by the average difference between the neutrino and muon directions. Based on [15], we take $\sigma_\alpha = 5^\circ$ for upward going muon events.

To account for the case that our estimates are not conservative enough, we will also consider a scenario where the resolutions are as poor as in Super-Kamiokande, and, in addition, the live time is taken to be only 250 days. On the other hand, we will also discuss a very optimistic setup with $\sigma_E/E = 2\%$ and $\sigma_\alpha = 2^\circ$ for contained events. In this setup, we also lower the energy threshold to 0.3 GeV and increase the exposure time to 2,000 days.

¹ This binning could not be employed in the analysis of real data, since the event numbers in each bin would be very small, but for our purposes, it gives a good estimate of the information that is contained in the data.

	ATLAS Realistic	ATLAS Cons.	ILC
Running time	500 d	250 d	2,000 d
Energy threshold	1.5 GeV	1.5 GeV	0.3 GeV
σ_E/E (contained events)	5%	17%	2%
σ_α (contained events)	7°	17°	2°
σ_α (upward muons)	5°	5°	5°
E bins	30	20	90
$\cos\theta$ bins (contained events)	36	10	80
$\cos\theta$ bins (upward muons)	27	27	27

Table I: Properties of the realistic and conservative ATLAS scenarios, and of an assumed ILC detector.

These assumptions will most probably not apply to ATLAS, since they would correspond to a situation where neutrino reconstruction is possible even during normal LHC operation, and the reconstruction efficiency is almost 100%. However, they may be interesting in the context of future projects such as the proposed ILC detectors [37]. In an ILC experiment, no pile-up of hadronic events will occur, so neutrino detection is not restricted to the maintenance phases of the accelerator. The parameters of our three scenarios are summarized in Tab. I

To analyze the simulated event spectra, we use a χ^2 fit which distinguishes neutrinos from anti-neutrinos, i.e. we assume 100% charge identification efficiency. For each species, we define a χ^2 function of the form

$$\chi_{\text{stat}}^2 = \sum_{i,j} 2 [T_{ij}(\vec{\Theta}_{\text{fit}}, \vec{a}) - N_{ij}(\vec{\Theta}_{\text{true}})] + 2 N_{ij}(\vec{\Theta}_{\text{true}}) \ln \left(\frac{N_{ij}(\vec{\Theta}_{\text{true}})}{T_{ij}(\vec{\Theta}_{\text{fit}}, \vec{a})} \right) + \chi_{\text{pull,osc}}^2 + \chi_{\text{pull,sys}}^2 \quad (5)$$

Here, $N_{ij}(\vec{\Theta}_{\text{true}})$ is the “observed” event rate in bin (i, j) for the “true” oscillation parameters $\vec{\Theta}_{\text{true}} = (\theta_{12}, \theta_{13}, \theta_{23}, \delta_{\text{CP}}, \Delta m_{21}^2, \Delta m_{31}^2, V)$, and $T_{ij}(\vec{\Theta}_{\text{fit}}, \vec{a})$ is the event rate that would be expected for the hypothesized parameters $\vec{\Theta}_{\text{fit}}$, and for biases \vec{a} arising from systematic errors in the experiment. We have introduced pull terms

$$\chi_{\text{pull,osc}}^2 = \sum_k \frac{(\Theta_{k,\text{fit}} - \Theta_{k,\text{true}})^2}{\sigma_{\Theta_k}^2}, \quad (6)$$

to account for external input on the oscillation parameters. σ_{Θ_k} determines how strongly a fit value far from the externally given one is disfavoured. Pull terms are provided only for those parameters which are marginalized over in the fit. We take relative 1σ uncertainties of 10% for θ_{12} and θ_{23} , 5% for Δm_{21}^2 , and 30% for Δm_{31}^2 . θ_{13} is assigned an absolute uncertainty of 10°.

Error Type	$\sigma_{\mathbf{a}}$
Overall normalization for contained events	20%
Relative normalization for anti-neutrinos	5%
Normalization for upward going muon events	20%
Tilt of E spectrum	5%
Tilt of θ spectrum for contained events	10%
Tilt of θ spectrum for upward going muon events	2%

Table II: Systematical errors in ATLAS.

Pull terms for systematical biases are similar to those for the oscillation parameters:

$$\chi_{\text{pull,sys}}^2 = \sum_k \frac{a_k^2}{\sigma_{a_k}^2}. \quad (7)$$

They disfavor fit values a_k which are further from zero than can be expected from the systematical uncertainties σ_{a_k} . We have defined \vec{a} such that the case of vanishing systematical errors corresponds to $\vec{a} = 0$. The various types of systematical errors we consider, are summarized in Tab. II. Besides the usual normalization errors we allow also for “tilts” in the event spectrum, which are a simple way of accounting for energy or angle dependent biases.

Note that many of the technical details of our simulations and of our statistical analysis procedure follow ideas that have been previously realized in the GLOBES code [38, 39].

5. SIMULATION RESULTS

In this section, we present our main results on the sensitivity of ATLAS to the leading atmospheric oscillation parameters and to three-flavor effects. In Fig. 1, we compare the expected confidence regions in the $\theta_{23}-\Delta m_{31}^2$ plane for the three scenarios introduced in Sec. 4, and in Fig. 2 we relate them to the results of a global three-flavor fit to existing atmospheric neutrino data [26, 40], and to the expected performance of T2K [41, 42, 43]. From the plots, we first notice that in all three scenarios, neutrino oscillations can be confirmed at better than 3σ , i.e. the case $\theta_{23} = 0$, $\Delta m_{31}^2 = 0$ can be ruled out. However, in the conservative case, the sensitivity is only marginal due to the limited statistics and resolutions, and could be easily spoiled by unfavorable statistical fluctuations in the real experiments.

The precision with which the mixing angle can be determined is poor in all three scenarios: Even in the optimistic ILC case, the uncertainty at 3σ is about $\pm 30\%$, which is still slightly worse than the current bound from Super-Kamiokande, K2K, and MINOS ($\sim 23\%$, cf. [26]). A measurement of θ_{23} in ATLAS is not competitive at all. The sensitivity to θ_{23} in atmospheric neutrinos comes mainly from the up-down asymmetry of the neutrino flux,

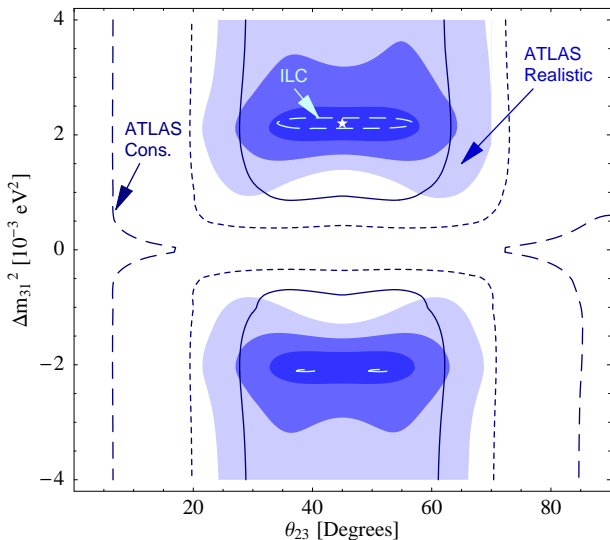


Figure 1: Sensitivity of ATLAS and of a possible ILC detector to the leading atmospheric oscillation parameters θ_{23} and Δm_{31}^2 . The shaded regions correspond to the 1σ , 2σ , and 3σ confidence levels for the realistic scenario, while the dark contours correspond to the conservative case. For the ILC scenario (light-colored contours), we show only the 3σ contour for clarity. A normal mass hierarchy has been assumed in the plot, but we have checked that all results except the sensitivity to the mass hierarchy, are similar for the inverted hierarchy (see text for details).

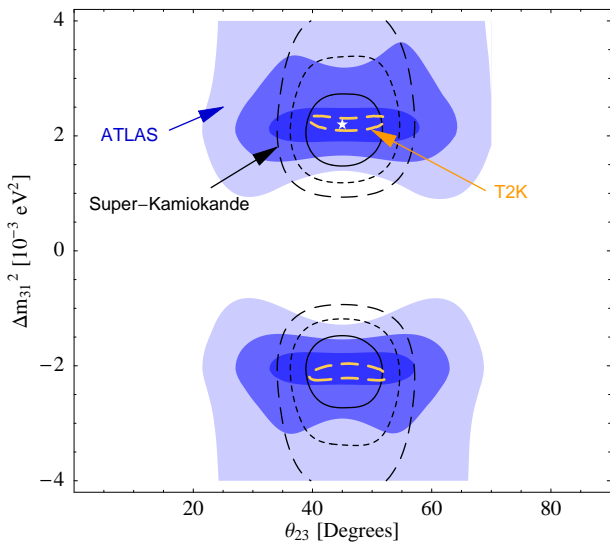


Figure 2: Sensitivity of ATLAS to the leading atmospheric oscillation parameters θ_{23} and Δm_{31}^2 in comparison with a global fit to existing atmospheric neutrino data (dominated by Super-Kamiokande) [26, 40], and with the expected performance of T2K. For the latter experiment, we show only the 3σ contour for clarity. A normal mass hierarchy was assumed in the plot, but we have checked that the results for the inverted hierarchy are analogous.

which can only be measured accurately with good statistics. The excellent resolution of ATLAS cannot compensate its small mass here.

The situation is better for Δm_{31}^2 : For the realistic scenario, ATLAS shows a performance similar to Super-Kamiokande, at least at low confidence levels. The 3σ contour, however, extends much further to large Δm_{31}^2 . In the ILC scenario, the sensitivity to Δm_{31}^2 is even comparable to that of T2K. An atmospheric neutrino oscillation experiment is sensitive to the mass squared difference mainly through the shape of the zenith angle spectrum at around $\cos\theta \approx 0$. These directions correspond to baselines below the first oscillation maximum, where the depletion of the flux is just setting in. Wash-out due to poor detector resolutions can greatly limit this measurement, so ATLAS-like detectors have a considerable advantage here.

Turning to the discovery potential for generic three-flavor effects, we remark, that although a very large value of $\sin^2 2\theta_{13} = 0.12$ was assumed in Fig. 1 and Fig. 2, the wrong hierarchy solution [44, 45] cannot be fully ruled out at 3σ even by an advanced ILC detector. In the two ATLAS scenarios, there is no sensitivity to the hierarchy at all. If the true hierarchy is inverted, matter effects are shifted to the anti-neutrino channels, where they are cloaked due to the smaller anti-neutrino cross sections, and we have checked that in this case, even the ILC scenario has only a 1σ discovery potential. One might have hoped that matter effects in the $\nu_\mu \rightarrow \nu_\mu$ channel could have helped to resolve this degeneracy [24, 25], but it turns out that the event numbers are too small in the relevant energy range of several GeV.

For the same reason, we also expect a poor performance in the investigation of other three-flavor effects. To demonstrate this, we have plotted in Fig. 3 the sensitivity of the realistic ATLAS scenario and several other experiments to $\sin^2 2\theta_{13}$. As examples for reactor experiments, we show Double CHOOZ [1], and a more advanced setup with a 200 t far detector [46]. On the accelerator side, we show simulation results for MINOS [47], T2K [4], and NO ν A [3, 48]. The sensitivity to $\sin^2 2\theta_{13}$ is defined as the limit, which a specific experiment can set to $\sin^2 2\theta_{13}$, assuming the true value is zero. The left edges of the bars correspond to the hypothetical case that only statistical errors are present in the experiment. The blue, green, and yellow bars reflect the limitations of the sensitivity due to systematical uncertainties, parameter correlations, and the $\text{sign}(\Delta m_{31}^2)$ degeneracy.² We can read off from Fig. 3 that atmospheric neutrino experiments can in general not compete with reactor and accelerator setups. Only Hyper-Kamiokande and the ILC scenario could improve the CHOOZ bound, though not as

² The octant degeneracy [45] is irrelevant here since we have assumed $\theta_{23}^{\text{true}} = \pi/4$, and the intrinsic degeneracy [49] appears only in high statistics experiments such as a neutrino factory.

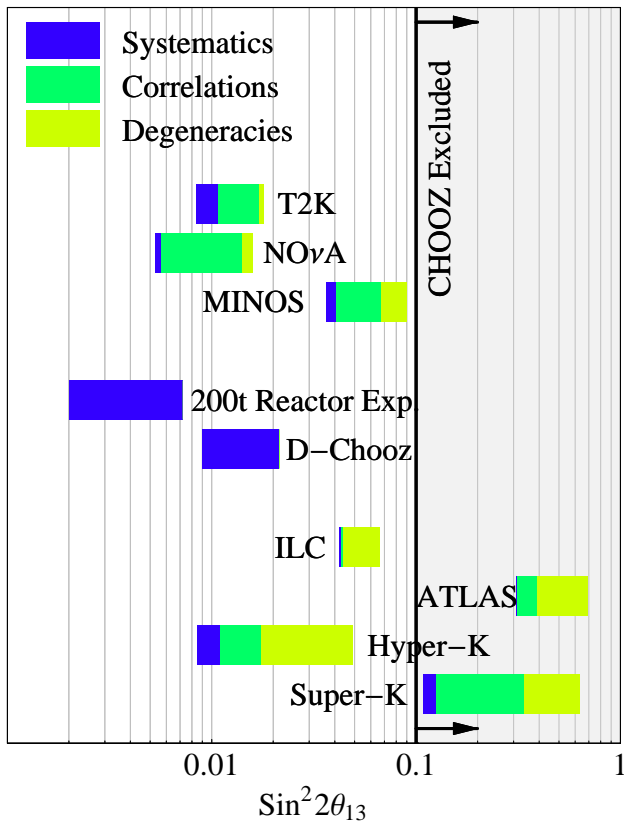


Figure 3: Sensitivity of various neutrino oscillation experiments to $\sin^2 2\theta_{13}$. The colored bars reflect the limitations of the sensitivity due to systematical errors, parameter correlations, and degeneracies. The right edges of the bars correspond to the sensitivity which is expected in reality.

much as dedicated experiments. It is interesting to note that the ILC scenario has a significantly better sensitivity than Super-Kamiokande, although it has only $\sim 1,350$ contained ν_μ events and $\sim 1,720$ upward going muons, while Super-Kamiokande has detected $\sim 4,500$ fully contained μ -like events and $\sim 2,250$ upward going muons, plus a large number of e -like events and partially contained events [15]. This comparison confirms the statement that, to a certain degree, excellent resolutions can compensate for low statistics in atmospheric neutrino experiments [12].

6. CONCLUSIONS

We have shown that atmospheric neutrino interactions are an interesting by-product of operating the ATLAS detector. Although reconstruction of these events is restricted to phases where the LHC is not running, or only running at low luminosity, the number of events, in conjunction with the expected good energy and angular resolutions, is sufficient to confirm atmospheric neutrino oscillations and to measure the leading oscillation parameters θ_{23} and Δm_{31}^2 . However, the precision of these

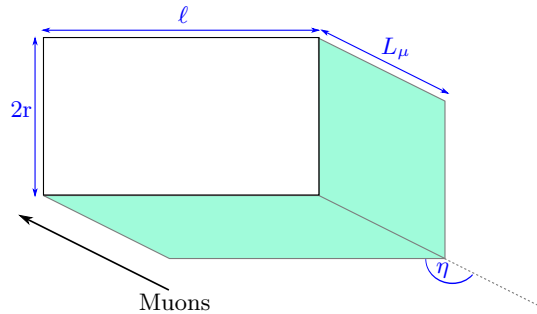


Figure 4: Geometry of upward going muons. The white rectangle schematically shows the ATLAS experiment as seen from a direction orthogonal to the detector axis and to the muon direction. The shaded region represents the effective target volume V .

measurements will probably not be competitive to that of existing and upcoming dedicated experiments. Under more optimistic assumptions, which might be realized at future ILC detectors, the errors on θ_{23} and Δm_{31}^2 can become comparable to those of T2K, and, if θ_{13} is very large, the $\text{sign}(\Delta m_{31}^2)$ degeneracy might be resolved at the 2σ level.

To study the reconstruction capabilities and sensitivities of ATLAS in more detail, it will be necessary to perform detailed detector Monte Carlo simulations. We believe this to be definitely worthwhile, since a measurement of the atmospheric neutrino oscillation parameters with the technology of ATLAS would be a very interesting result in itself, even if the final error bars should be larger than those of other experiments. Moreover, the exploration of neutrino interactions in ATLAS would provide valuable experience that could be of great interest in the design of future collider experiments and neutrino detectors.

Acknowledgments

We would like to thank E. Kh. Akhmedov, S. Goswami, K. A. Hochmuth, P. Huber, J. Schmaler, W. Smith, and especially F. Vannucci for useful discussions. We are especially grateful to T. Schwetz-Mangold for kindly providing the results of the global fit to atmospheric neutrino data from [26, 40] in machine-readable form. JK would like to acknowledge support from the Studienstiftung des Deutschen Volkes.

Appendix A: GEOMETRY OF UPWARD GOING MUONS IN ATLAS

As mentioned in Sec. 4, the target volume for upward going muon events depends on the energy and on the zenith and azimuthal angles. It can be calculated from geometrical arguments as follows. We first integrate the

inverse of the Bethe-Bloch formula [50, 51] to obtain the “muon range” L_μ , i.e. the average distance that a muon with energy E_μ can travel in rock. We then use Fig. 4 to calculate the effective target volume V in which a neutrino must interact to induce an upward going muon event in the detector. The white rectangle in the diagram represents the cylindrical ATLAS detector as seen from a direction orthogonal to the detector axis and to the muon direction, so that the angle η between these two vectors lies in the drawing plane. The effective target volume, shown by the shaded region in Fig. 4, is given by

$$V = L_\mu |\sin \eta| \cdot \ell \cdot 2r + L_\mu |\cos \eta| \cdot \pi r^2. \quad (\text{A1})$$

We can calculate η from the azimuthal angle ϕ and the zenith angle θ by

$$\cos \eta = \sin \theta \cos \phi. \quad (\text{A2})$$

Averaging over ϕ yields

$$\begin{aligned} \bar{V} &= \frac{L_\mu}{2\pi} \int_0^{2\pi} d\phi (2r\ell \sqrt{1 - \sin^2 \theta \cos^2 \phi} + \pi r^2 |\sin \theta \cos \phi|) \\ &= \frac{4r\ell L_\mu}{\pi} E(\sin \theta) + 2r^2 L_\mu |\sin \theta|, \end{aligned} \quad (\text{A3})$$

with $E(\cdot)$ being the complete elliptic integral of the second kind [52].

When evaluating this expression, we assume a horizontally cylindrical geometry for ATLAS, with a length of 42 m and a radius of 11 m. For the geometrical arguments, the muon direction is taken to be identical to that of the primary neutrino, which is justified by the fact that upward going muons typically have very high energies $\gg 1$ GeV. The muon energy is calculated from the neutrino energy according to the empirical formula

$$E_\mu = E_\nu \left(e^{5.255 - 1.819 \log_{10}(E_\nu/\text{MeV})} + 0.3298 \right), \quad (\text{A4})$$

which we have obtained by fitting E_μ/E_ν in a sample of 1,000 upward going muon events in Super-Kamiokande, simulated with the NUANCE event generator [53].

-
- [1] F. Ardellier et al. (Double Chooz) (2006), hep-ex/0606025.
- [2] X. Guo et al. (Daya Bay) (2007), hep-ex/0701029.
- [3] D. S. Ayres et al. (NOvA) (2004), hep-ex/0503053.
- [4] K. Nishikawa et al. (T2K) (2006), URL http://j-parc.jp/NuclPart/pac_0606/pdf/p11-Nishikawa.pdf.
- [5] K. Nakamura, Int. J. Mod. Phys. **A18**, 4053 (2003).
- [6] G. Rajasekaran, AIP Conf. Proc. **721**, 243 (2004), hep-ph/0402246.
- [7] P. Huber, M. Lindner, M. Rolinec, and W. Winter, Phys. Rev. **D73**, 053002 (2006), hep-ph/0506237.
- [8] P. Zucchelli, Phys. Lett. **B532**, 166 (2002).
- [9] S. Geer, Phys. Rev. **D57**, 6989 (1998), hep-ph/9712290.
- [10] P. Huber, M. Lindner, M. Rolinec, and W. Winter, Phys. Rev. **D74**, 073003 (2006), hep-ph/0606119.
- [11] F. Vannucci, private communication.
- [12] S. T. Petcov and T. Schwetz (2005), hep-ph/0511277.
- [13] Y. Fukuda et al. (Super-Kamiokande), Phys. Rev. Lett. **81**, 1562 (1998), hep-ex/9807003.
- [14] Y. Ashie et al. (Super-Kamiokande), Phys. Rev. Lett. **93**, 101801 (2004), hep-ex/0404034.
- [15] Y. Ashie et al. (Super-Kamiokande), Phys. Rev. **D71**, 112005 (2005), hep-ex/0501064.
- [16] E. Aliu et al. (K2K), Phys. Rev. Lett. **94**, 081802 (2005), hep-ex/0411038.
- [17] D. G. Michael et al. (MINOS), Phys. Rev. Lett. **97**, 191801 (2006), hep-ex/0607088.
- [18] O. L. G. Peres and A. Y. Smirnov, Phys. Lett. **B456**, 204 (1999), hep-ph/9902312.
- [19] M. Honda, T. Kajita, K. Kasahara, and S. Midorikawa, Phys. Rev. **D70**, 043008 (2004), astro-ph/0404457.
- [20] G. Battistoni, A. Ferrari, T. Montaruli, and P. R. Sala, Astropart. Phys. **19**, 269 (2003), hep-ph/0207035.
- [21] G. Battistoni, A. Ferrari, T. Montaruli, and P. R. Sala (2003), hep-ph/0305208.
- [22] G. D. Barr, T. K. Gaisser, P. Lipari, S. Robbins, and T. Stanev, Phys. Rev. **D70**, 023006 (2004), astro-ph/0403630.
- [23] E. K. Akhmedov, R. Johansson, M. Lindner, T. Ohlsson, and T. Schwetz, JHEP **04**, 078 (2004), hep-ph/0402175.
- [24] R. Gandhi, P. Ghoshal, S. Goswami, P. Mehta, and S. Uma Sankar, Phys. Rev. Lett. **94**, 051801 (2005), hep-ph/0408361.
- [25] R. Gandhi, P. Ghoshal, S. Goswami, P. Mehta, and S. Uma Sankar (2004), hep-ph/0411252.
- [26] M. Maltoni, T. Schwetz, M. A. Tortola, and J. W. F. Valle, New J. Phys. **6**, 122 (2004), hep-ph/0405172.
- [27] G. L. Fogli, E. Lisi, A. Marrone, and A. Palazzo, Prog. Part. Nucl. Phys. **57**, 742 (2006), hep-ph/0506083.
- [28] J. N. Bahcall, M. C. Gonzalez-Garcia, and C. Pena-Garay, JHEP **08**, 016 (2004), hep-ph/0406294.
- [29] A. Bandyopadhyay, S. Choubey, S. Goswami, S. T. Petcov, and D. P. Roy, Phys. Lett. **B608**, 115 (2005), hep-ph/0406328.
- [30] W. W. Armstrong et al. (ATLAS) (1994), CERN-LHCC-94-43.
- [31] P. Collier, Tech. Rep., CERN (2004), summary of several talks given at 1st LHC Project Workshop Chamonix XIII, Chamonix, France, 19-23 Jan 2004, URL <http://cdsweb.cern.ch/record/725413>.
- [32] The CMS collaboration (CMS) (1994), CERN-LHCC-94-38.
- [33] W. M. Yao et al. (Particle Data Group), J. Phys. **G33**, 1 (2006).

- [34] M. D. Messier, Ph.D. thesis, Boston University (1999), UMI-99-23965.
- [35] E. A. Paschos and J. Y. Yu, Phys. Rev. **D65**, 033002 (2002), hep-ph/0107261.
- [36] M. Ishitsuka, Ph.D. thesis, Tokyo University (2004).
- [37] Tech. Rep. (2007), URL <http://physics.uoregon.edu/~lc/wwstudy/>.
- [38] P. Huber, M. Lindner, and W. Winter, Comput. Phys. Commun. **167**, 195 (2005), hep-ph/0407333, URL <http://www.mpi-hd.mpg.de/~globes>.
- [39] P. Huber, J. Kopp, M. Lindner, M. Rolinec, and W. Winter (2007), hep-ph/0701187, URL <http://www.mpi-hd.mpg.de/~globes>.
- [40] T. Schwetz, Phys. Scripta **T127**, 1 (2006), hep-ph/0606060.
- [41] Y. Itow et al. (2001), hep-ex/0106019.
- [42] P. Huber, M. Lindner, and W. Winter, Nucl. Phys. **B645**, 3 (2002), hep-ph/0204352.
- [43] M. Ishitsuka, T. Kajita, H. Minakata, and H. Nunokawa, Phys. Rev. **D72**, 033003 (2005), hep-ph/0504026.
- [44] H. Minakata and H. Nunokawa, JHEP **10**, 001 (2001), hep-ph/0108085.
- [45] V. Barger, D. Marfatia, and K. Whisnant, Phys. Rev. **D65**, 073023 (2002), hep-ph/0112119.
- [46] P. Huber, J. Kopp, M. Lindner, M. Rolinec, and W. Winter (2006), hep-ph/0601266.
- [47] E. Ables et al. (MINOS) (1995), FERMILAB-PROPOSAL-P-875.
- [48] T. Yang and S. Wojcicki (NOvA) (2004), Off-Axis-Note-SIM-30.
- [49] J. Burguet-Castell, M. B. Gavela, J. J. Gomez-Cadenas, P. Hernandez, and O. Mena, Nucl. Phys. **B608**, 301 (2001), hep-ph/0103258.
- [50] S. Eidelman et al. (Particle Data Group), Phys. Lett. **B592**, 1 (2004).
- [51] D. E. Groom, N. V. Mokhov, and S. I. Striganov, Atom. Data Nucl. Data Tabl. **78**, 183 (2001).
- [52] M. Abramowitz and I. A. Stegun, *Handbook of Mathematical Functions with Formulas, Graphs, and Mathematical Tables* (Dover, New York, 1964), ninth dover printing, tenth gpo printing ed., ISBN 0-486-61272-4.
- [53] D. Casper, Nucl. Phys. Proc. Suppl. **112**, 161 (2002), hep-ph/0208030.